

Article

Dielectric Properties and Magnetoelectric Effect of $\text{Bi}_7\text{Fe}_3\text{Ti}_3\text{O}_{21}$ Ceramic Material Doped with Gadolinium Ions

Diana Szalbot ¹, Joanna A. Bartkowska ¹, Jolanta Makowska ¹, Maciej Chrunik ², Katarzyna Osińska ¹ and Małgorzata Adamczyk-Habrajska ^{1,*}

¹ Faculty of Science and Technology, Institute of Materials Engineering, University of Silesia, 75 Pułku Piechoty 1A, 41-500 Chorzow, Poland; diana.szalbot@gmail.com (D.S.); joanna.bartkowska@us.edu.pl (J.A.B.); jolanta.makowska@us.edu.pl (J.M.); katarzyna.osinska@us.edu.pl (K.O.)

² Institute of Applied Physics, Military University of Technology, 2 Gen. Sylwestra Kaliskiego St., 00-908 Warsaw, Poland; maciej.chrunik@wat.edu.pl

* Correspondence: malgorzata.adamczyk-habrajska@us.edu.pl; Tel.: +48-32-2691841

Abstract: Pure $\text{Bi}_7\text{Fe}_3\text{Ti}_3\text{O}_{21}$ ceramic material and gadolinium ion (Gd^{3+})-doped ones were prepared by solid-state reaction method using simple oxides. The findings of the XRD measurements confirmed the initial author's assumption that the dopant ions substituted in perovskite blocks influenced the dimensions of the unit cell parameters. All obtained materials are single-phase and show an orthorhombic structure with the $Fm2m$ space group. Microstructure studies show that the admixture gadolinium doping changes the microstructure of the base material, changing grain shapes from plate-like to rounded. The temperature dependences of the electric permittivity have shown the existence of a maximum, the temperature location of which depends on both the frequency and the concentration of Gd^{3+} ions. The highest values of electric permittivity were characteristic of the material with an admixture of Gd^{3+} ions in the amount of $x = 0.6$ ($f = 1$ kHz), and the lowest values were for material with $x = 0.2$ ($f = 1$ kHz). Studies of the magnetoelectric effect have shown that the strongest coupling between magnetic and electrical properties was demonstrated by a material doped with Gd^{3+} ions in the amount of $x = 0.2$, for which the magnetoelectric coupling coefficient is equal to $\alpha = 12.58 \cdot 10^{-9}$ s/m.

Keywords: magnetoelectric coupling coefficient; Aurivillius phases; dielectric properties



Citation: Szalbot, D.; Bartkowska, J.A.; Makowska, J.; Chrunik, M.; Osińska, K.; Adamczyk-Habrajska, M. Dielectric Properties and Magnetoelectric Effect of $\text{Bi}_7\text{Fe}_3\text{Ti}_3\text{O}_{21}$ Ceramic Material Doped with Gadolinium Ions. *Appl. Sci.* **2024**, *14*, 3920. <https://doi.org/10.3390/app14093920>

Academic Editor: Andrea Carpinteri

Received: 5 April 2024

Revised: 28 April 2024

Accepted: 1 May 2024

Published: 4 May 2024



Copyright: © 2024 by the authors. Licensee MDPI, Basel, Switzerland. This article is an open access article distributed under the terms and conditions of the Creative Commons Attribution (CC BY) license (<https://creativecommons.org/licenses/by/4.0/>).

1. Introduction

In recent years, the scientific community has observed a growing interest in multiferroic materials, driven by their unique physical properties and promising applications. These materials are distinguished by the simultaneous presence of electric and magnetic fields, a characteristic stemming from their multiferroicity. This dual nature makes them suitable for advanced sensors and multi-state memory systems [1–6]. The drive towards sustainable technology solutions has also placed multiferroics at the forefront of energy harvesting and photocatalysis research [7]. The ability of these materials to manipulate photo-generated charge carriers through their internal fields presents an innovative approach to enhancing the efficiency of solar energy devices [7–10]. Notably, there is a specific emphasis on the quest for materials exhibiting the magnetoelectric effect, measured by the magnetoelectric coupling coefficient. This coefficient determines how strong the coupling between magnetic and electrical properties is [11,12]. Multiferroics include various materials, among which an important group that has attracted great interest in recent years is materials with the Aurivillius-type structure [13,14]. These materials are characterized by the general formula $(\text{M}_2\text{O}_2)^{2+}(\text{A}_{m-1}\text{B}_m\text{O}_{3m+1})^{2-}$, where the M position is predominantly occupied by bismuth ions [15,16]. The formulation indicates that these compounds consist of systematically arranged $(\text{Bi}_2\text{O}_2)^{2+}$ layers and perovskite blocks $(\text{A}_{m-1}\text{B}_m\text{O}_{3m+1})^{2-}$, with the parameter m denoting the number of such blocks situated between the bismuth oxides layers [17].

The distinctive crystal lattice and intriguing physical properties of these materials are contingent upon the value of the Aurivillius phase number m [13,18].

The research focused on $\text{Bi}_7\text{Fe}_3\text{Ti}_3\text{O}_{21}$ ceramics within the $\text{Bi}_4\text{Ti}_3\text{O}_{12}$ - BiFeO_3 system, incorporating varying concentrations of gadolinium ions (Gd^{3+}). The premise was that these dopant ions would replace the $(\text{A}_{m-1}\text{B}_m\text{O}_{3m+1})^{2-}$ structures within the perovskite blocks at the A position. Technological conditions, established through solid-state synthesis from simple oxides, were employed to synthesize novel ceramic materials $\text{Bi}_{7-x}\text{Gd}_x\text{Fe}_3\text{Ti}_3\text{O}_{21}$ with x values of (0, 0.2, 0.4, 0.6) (BGFT- x). Considering the ionic radii of gadolinium and bismuth (Table 1) [19], it was postulated that the substitution would alter the unit cell parameters, thereby influencing the inherent material properties. Subsequent measurements validated this hypothesis, revealing a modification in electric permittivity. The primary focus was on scrutinizing the impact of the modifier (Gd^{3+}) on the electromagnetic coupling values within the tested multiferroic materials.

Table 1. Comparison of the basic information about gadolinium and bismuth ions [19].

| | Valence | Coordination Number | Ionic Radii Å [19] |
|------------------|---------|---------------------|--------------------|
| Gd^{3+} | III | 6 | 0.94 |
| Bi^{3+} | III | 6 | 1.03 |

2. Materials and Methods

The preparation of pure $\text{Bi}_7\text{Fe}_3\text{Ti}_3\text{O}_{21}$ ceramic material and its gadolinium ion (Gd^{3+})-doped counterpart was accomplished through the solid-state reaction method, utilizing simple oxides. The procedural details are explained in our previous paper [20,21]. Figure 1 shows general scheme. To identify suitable synthesis parameters, the preliminary-mixed powders underwent thermal analysis (TG, DTG, DTA) within the temperature range $T = (298\text{--}1298)$ K. The resulting data facilitated the determination of the synthesis temperature for all compounds, established at $T_s = 1123$ K.

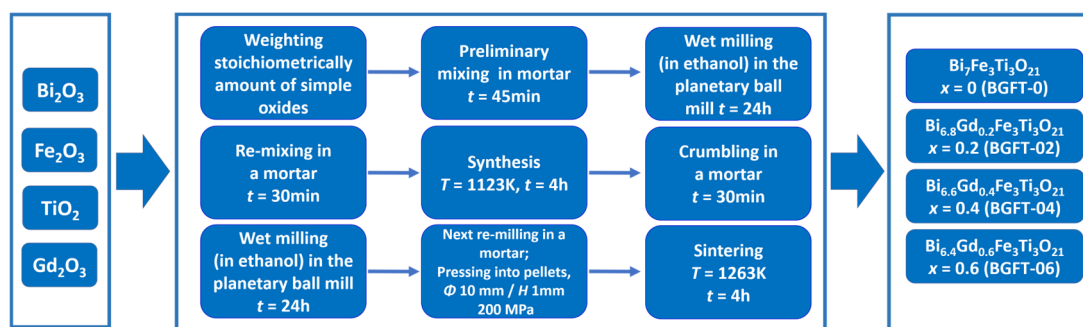


Figure 1. General fabrication scheme for BGFT- x ceramic materials (for $x = (0, 0.2, 0.4, 0.6)$).

The crystal structures of all examined samples were investigated using a BRUKER D8 Discover instrument equipped with a standard $\text{CuK}\alpha$ radiator ($\lambda\text{K}\alpha_1 = 1.54056$ Å, $\lambda\text{K}\alpha_2 = 1.54439$ Å, Siemens KFL CU2 K, operating at 40 kV voltage and 40 mA current in the Bragg-Brentano diffraction geometry with a Göbel FGM2 mirror for parallel beam conditions). The diffraction angle 2θ range was set from $15\text{--}80^\circ$ with a step of 0.015° and an acquisition time of 2 s per step. All measurements were conducted at 298 K within the temperature-stabilized Anton Paar HTK 1200N chamber. Data processing involved the use of the Crystal Impact Match! application. The $\lambda\text{K}\alpha_2$ signal component was deconvoluted and removed for each diffraction pattern, the background was subtracted, and the data were smoothed using the fast Fourier transform. The phase analysis was performed using the ICSD database. Crystallographic calculations were performed by means of the FullPROF ver. 3.0 program, enabling Rietveld refinement and precise unit cell parameter calculations based on diffraction profile fitting [22]. The reference CIF file used for this analysis was

obtained from the supplementary data in Ref. [23]. The calculated broadening of diffraction lines, specifically the full width at half maximum (FWHM), was employed to estimate the average crystallite sizes using the Debye–Scherrer formula [24]. The instrumental standard NIST SRM 660a (LaB₆) was applied to eliminate the apparatus broadening component.

The microstructure analysis was conducted using a scanning electron microscope (JEOL JSM-7100F TTL LV) equipped with an energy dispersion spectrometer (EDS). Qualitative and quantitative assessments of the chemical composition were performed employing the X-ray microanalysis method.

Dielectric measurements were conducted using the Agilent E4980A impedance analyzer within a frequency range spanning from $f = 1$ kHz to $f = 1000$ kHz and at temperatures ranging from $T = 300$ K to $T = 800$ K. The measurements were carried out during the heating and cooling processes, with the rate of $V = 2.5$ K/min, and stabilised using a temperature controller. An Agilent E4980A LCR meter was used to measure the dielectric response.

3. Results and Discussion

3.1. X-ray Diffraction

To determine the crystal structure of the $\text{Bi}_{7-x}\text{Gd}_x\text{Fe}_3\text{Ti}_3\text{O}_{21}$ (BGFT- x) for $x = (0, 0.2, 0.4, 0.6)$, X-ray analysis was conducted. The obtained XRD patterns (Figure 2) indicate that the examined ceramic materials are single-phase and exhibit the anticipated orthorhombic structure with the $\text{Fm}2\text{m}$ (No. 42) space group. The exemplary profile fitting is shown in Figure 3.

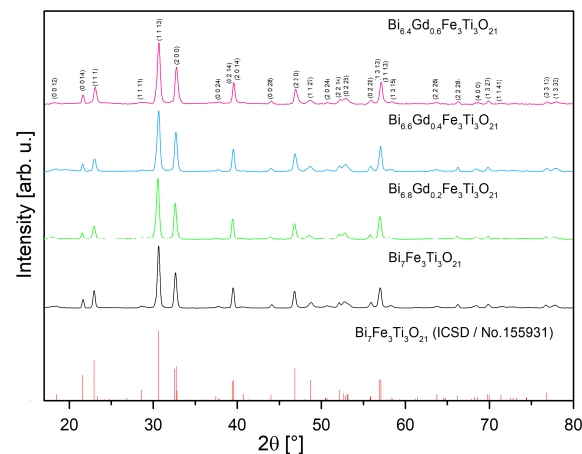


Figure 2. A set of experimental diffraction patterns of obtained BGFT- x ($x = (0, 0.2, 0.4, 0.6)$) powders with reference ICSD pattern of Aurivillius phase.

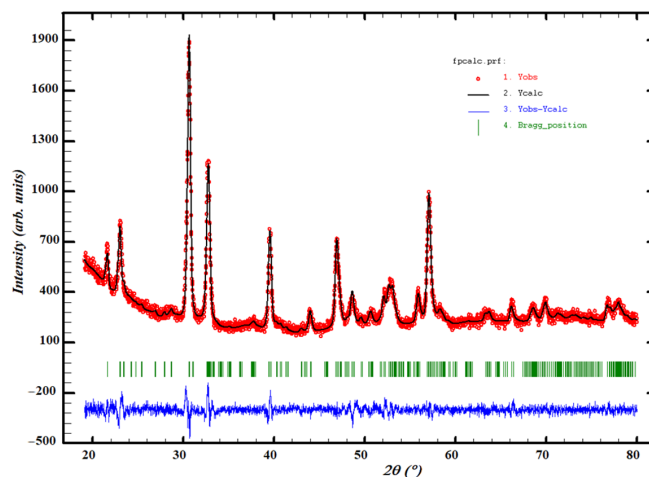


Figure 3. An exemplary pattern obtained from Rietveld refinement of $\text{Bi}_{6.4}\text{Gd}_{0.6}\text{Fe}_3\text{Ti}_3\text{O}_{21}$ powders (generated from WinPlotr).

The parameters of the unit cell of the discussed ceramic materials were determined from the structural analysis on the basis of XRD data. The results are presented in Table 2.

Table 2. Theoretical molar masses, refined lattice constants, unit cell volumes and theoretically calculated densities of obtained BGFT- x ($x = (0, 0.2, 0.4, 0.6)$) powders with reference to CIF file taken from Ref. [23]. The χ^2 factor is referred to Rietveld refinement.

| Source | x | M_{mol} [g/mol] | a [Å] | b [Å] | c [Å] | V [Å ³] | ρ [g/cm ³] | χ^2 |
|-----------|-----|-----------------------------|-----------|-----------|-----------|-----------------------|-----------------------------|----------|
| Ref. [23] | 0 | 2109.986 | 5.4699(3) | 5.4924(3) | 57.551(3) | 1729.0(2) | 8.106(1) | 6.50 |
| | | 2109.986 | 5.4837(2) | 5.4970(4) | 57.447(4) | 1731.7(2) | 8.0932(7) | 2.34 |
| This work | 0.2 | 2099.640 | 5.4725(3) | 5.4858(4) | 57.531(4) | 1727.2(2) | 8.0747(8) | 1.99 |
| | 0.4 | 2089.294 | 5.4773(3) | 5.5026(4) | 57.574(5) | 1735.2(2) | 7.9975(9) | 1.68 |
| | 0.6 | 2078.948 | 5.4695(3) | 5.4978(5) | 57.591(8) | 1731.8(3) | 7.974(2) | 1.47 |

The results of XRD studies and structure calculations revealed that the Aurivillius phase showed the ability to be doped with Gd³⁺ ions. There are at least a few arguments as to this. In every single case of x , we observe phase-homogeneous XRD diffractograms. Apart from the target phase of Aurivillius, neither substrate residues nor intermediate phases from the equilibrium system consisted of bismuth, iron, titanium, gadolinium oxides, or other noted inclusions were noted. The content of such diffractograms is only a diffraction pattern of the BGFT- x ($x = (0, 0.2, 0.4, 0.6)$) system, differing only in subtle changes in the positions of Bragg lines profiles, which is the result of changes in the lattice constants. Analyzing the unit cell parameters, it is noticed that their volume changes tend to increase with respect to the dopant content. With an increase in the gadolinium level, for the adopted concentration range (from $x = 0.2$ to $x = 0.6$), the volume of the BGFT- x unit cell increases slightly for $x = 0.4$, and the elongation of the lattice constant (b) is accompanied by less commensurate shortening of the lattice constant (a), while neither directional nor significant changes in the constant (c) are found (Table 2). Moreover, the increasing concentration of gadolinium ions Gd³⁺ causes a slight but gradual decrease in the theoretical density of the tested ceramic materials (calculated based on Formula (1)) (Table 2). The densities were calculated according to the formula given below:

$$\rho = \frac{MZ}{VN_A} \quad (1)$$

where M —molar mass of BGFT- x system, Z —the number of cell formula units (equal to 4 in each case), V —volume of unit cell, N_A —the Avogadro constant.

It should be emphasized that the valence of gadolinium ions is identical to that of bismuth, so there is no risk of oxygen defects, and gadolinium would theoretically take the nodal position of bismuth in the unit cell. According to the assumptions, the doping was meant to substitute bismuth with gadolinium and maintain the total stoichiometry resulting from the valence of these elements. The nature of the bonds of bismuth and gadolinium with oxygen within this cell could be controversial here because the atomic radius of gadolinium is larger than that of bismuth (233 and 143 pm, respectively), while the relation of their ionic radii is exactly the opposite (here 94 and 103 pm) but also shows better compatibility in the latter case. Since the unit cell's expansion (albeit insignificant) takes place, this may suggest that in the BGFT- x systems; however, the proportion of atomic bonds is higher than ionic ones. However, the electronegativity difference between Gd and O is 2.24, according to the Pauling scale, and only together with Ti (with a corresponding difference of 1.9) it does meet the necessary condition for the formation of ionic bonds—while both Bi and Fe have this parameter lower than 1.7—hence, the higher probability for creation of atomic bonds (and, thus, the domination of atomic instead of ionic radii in the formation of appropriate bonds). Additionally, the analysis of results is hampered by the fact that the Aurivillius phase belongs

to the disordered structures type. For this reason, the precise packing factor of a unit cell is practically impossible to determine. If this were a fixed parameter, then perhaps it would be easier to assess the possibility of dopants being incorporated into interstitial gaps as well—the Aurivillius phase, possessing a high volume of its unit cell, has many of them. In any case, the charge density distribution within the atomic orbitals is not an obstacle to doping the Aurivillius phase with gadolinium.

3.2. Scanning Electron Microscopy and X-ray Microanalysis (EDS)

Scanning electron microscopy (SEM) images depicting the fracture morphology of BGFT-0 ceramics, as well as the corresponding ceramics doped with gadolinium ions, are illustrated in Figure 4 for two different magnifications, namely 1000 times and 8000 times.

As already noted in previous publications [20,21], the grains of the base BGFT-0 ceramics exhibit a plate-like shape consistent with the characteristic morphology of compounds containing Aurivillius phases. The closely packed plates, overlapping each other, contribute to the formation of fractures that traverse through the grains during the fracture process. This phenomenon indicates the presence of well-sintered and robust grains with distinctly defined grain boundaries. Incorporating gadolinium Gd^{3+} admixture induces a significant transformation in the microstructure appearance of the examined fractured ceramic materials. In the case of BGFT-02, there is a noticeable alteration in the plate shapes, transitioning to rounded forms, and the distribution of grains becomes rather chaotic. Notably, the introduction of gadolinium results in a gradual reduction in the number of pores within the doped ceramics, correlating with the increased dopant content. The grain size across all ceramics exhibits heterogeneity. Particularly in the BGFT-02 material, the presence of individual large plates becomes apparent, with their proportion in the total grain count escalating as the Gd^{3+} modifier content increases.

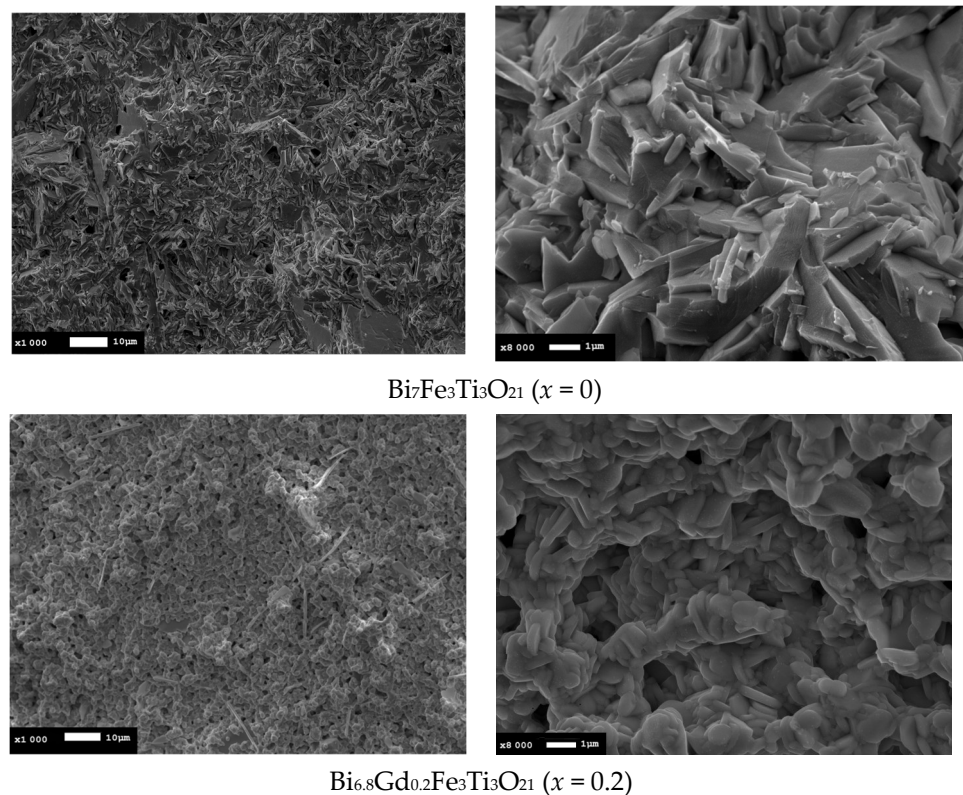


Figure 4. Cont.

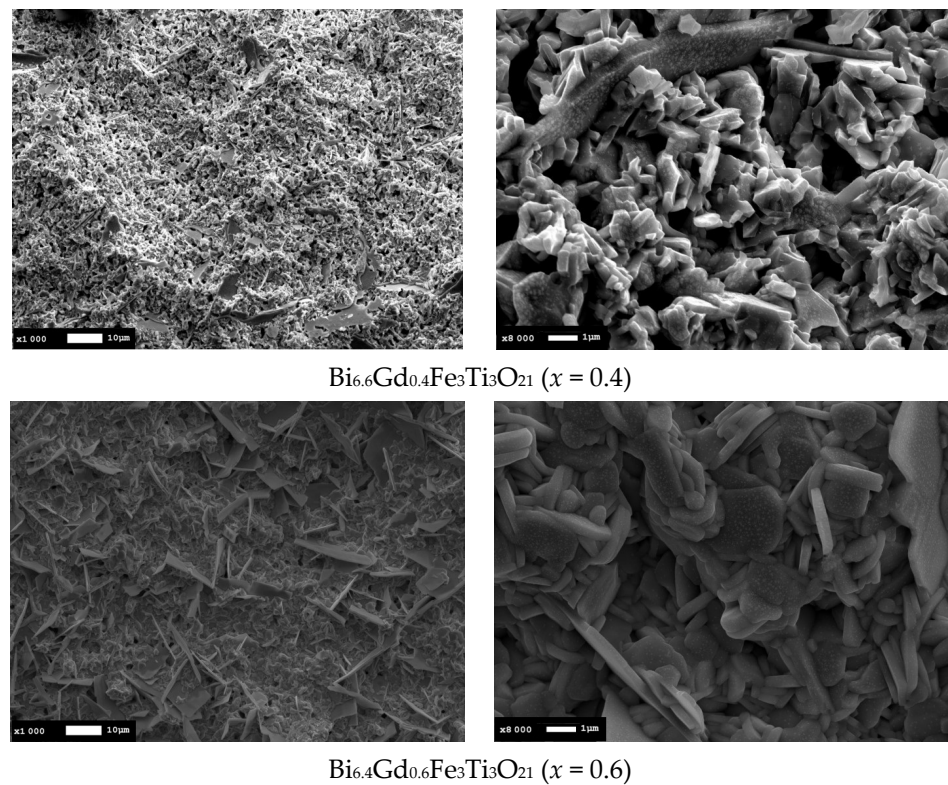


Figure 4. Microstructure of $\text{Bi}_{7-x}\text{Gd}_x\text{Fe}_3\text{Ti}_3\text{O}_{21}$ ceramic materials for $x = (0, 0.2, 0.4, 0.6)$.

The examined ceramic materials underwent energy-dispersive X-ray analysis (EDS). The measurements ruled out the presence of any foreign elements or impurities. An exemplary EDS spectrum, illustrated for the BGFT-06 ceramics sample, is presented in Figure 5.

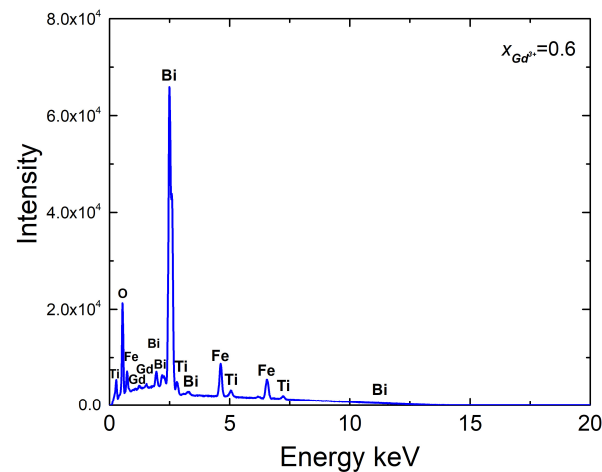


Figure 5. Exemplary EDS spectrum on the BGFT-06 ceramics.

The percentage composition of individual elements (calculated as oxides) in the examined materials is detailed in Table 3. For all obtained materials, a microanalysis of the chemical composition validated the theoretical stoichiometry assumed at the onset of the technological process. Minor deviations of the marked (actual) values from theoretical values fall within the measurement uncertainty range of the employed method.

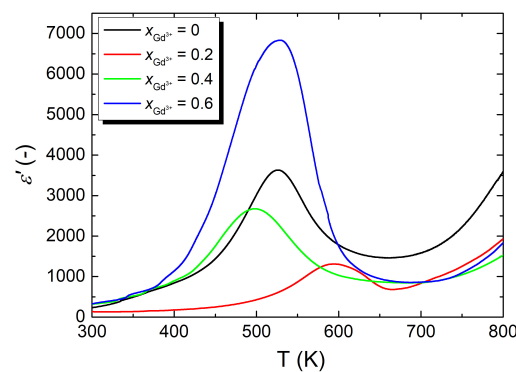
Table 3. Theoretical and experimental oxide percentage values for BGFT-x ceramic materials ($x = 0.2, 0.4, 0.6$).

| Gd ³⁺ | BGFT-x | | | |
|------------------|--------------------------------|-------------------------------|---|---|
| | Oxide Formula | Theoretical Oxide Content (%) | Determined Oxide Content from EDS (mag. 1000) (%) | The Difference between the Theoretical and Determined Oxide Content (%) |
| $x = 0.2$ | Bi ₂ O ₃ | 76 | 77 | 1 |
| | Gd ₂ O ₃ | 2 | 3 | 1 |
| | TiO ₂ | 11 | 10 | 1 |
| | Fe ₂ O ₃ | 11 | 10 | 1 |
| $x = 0.4$ | Bi ₂ O ₃ | 74 | 75 | 1 |
| | Gd ₂ O ₃ | 3 | 5 | 2 |
| | TiO ₂ | 12 | 10 | 2 |
| | Fe ₂ O ₃ | 11 | 10 | 1 |
| $x = 0.6$ | Bi ₂ O ₃ | 72 | 72 | 0 |
| | Gd ₂ O ₃ | 5 | 7 | 2 |
| | TiO ₂ | 12 | 10 | 2 |
| | Fe ₂ O ₃ | 11 | 11 | 0 |

3.3. Dielectric Properties

In order to perform dielectric measurements, the samples were first subjected to a preparatory process. After the grinding of the samples was completed, they were subjected to a stress-relief annealing process to remove the structural stresses resulting from grinding. The process took place in a muffle furnace at the temperature of $T = 723$ K for $t = 2$ h. The samples were then cooled to room temperature. Before applying the electrodes, the disks were degreased in ethyl acetate, and then the electrodes were applied using hot platinum paste. Samples with electrodes applied were dried at a temperature of $T = 473$ K for $t = 0.5$ h in an SML 30–250 dryer and then fired in a muffle furnace at a temperature of $T = 1123$ K for $t = 0.5$ h.

In order to investigate the dielectric properties of the Bi₇Fe₃Ti₃O₂₁ base ceramics doped with gadolinium ions, the characteristics of the electrical permittivity versus the temperature were determined and measured in a measurement field with frequencies in the $f = (1–1000)$ Hz range. Figure 6 shows the temperature characteristics of the real part of the electrical permittivity of Bi_{7–x}Gd_xFe₃Ti₃O₂₁ ceramics for $x = (0, 0.2, 0.4, 0.6)$, which were measured in a measurement field of $f = 1$ kHz, in the temperature range $T = (300–800)$ K.

**Figure 6.** Temperature characteristics of the real part of electrical permittivity measured in Bi_{7–x}Gd_xFe₃Ti₃O₂₁ ceramic materials for $x = (0, 0.2, 0.4, 0.6)$ in a measurement field with a frequency of $f = 1$ kHz.

The gadolinium dopant induces indiscriminate changes in both the values of electrical permittivity, particularly its maximum value and the temperature at which its maximum occurs. Adding a dopant at a level of $x = 0.2$ results in a decrease in ϵ'_{max} and a shift in the temperature of its occurrence T_{max} towards higher values. Conversely, for a dopant level of $x = 0.4$, ϵ'_{max} increases again while its temperature shifts towards lower values. Furthermore, increasing the concentration of the modifier to $x = 0.6$ leads to a sharp increase in the value of the real part of permittivity to values exceeding 6000. The corresponding temperature T_{max} has practically the same value as in the case of the pure $\text{Bi}_7\text{Fe}_3\text{Ti}_3\text{O}_{21}$ compound (Table 4).

Table 4. Electrical parameters measured in the measurement field $f = 1$ kHz for $\text{Bi}_{7-x}\text{Gd}_x\text{Fe}_3\text{Ti}_3\text{O}_{21}$ ceramic materials for $x = (0, 0.2, 0.4, 0.6)$.

| x | $\text{Bi}_{7-x}\text{Gd}_x\text{Fe}_3\text{Ti}_3\text{O}_{21}$ T_{max} [K] | ϵ'_{max} |
|-----|--|-------------------|
| 0 | 524 | 3623 |
| 0.2 | 579 | 1312 |
| 0.4 | 498 | 2674 |
| 0.6 | 529 | 6835 |

The addition of gadolinium ions significantly influenced the microstructure, causing grain growth and increasing their size non-uniformity. On the other hand, we also observe its effect on the electrical permittivity, raising the question: what truly accounts for the changes in dielectric properties? Is it the dopant or the change in grain size? This is a serious issue. On the one hand, in the literature, we find many examples of grain size affecting dielectric properties, especially extensively described for BaTiO_3 [25,26]. On the other hand, introducing dopant ions into the lattice also affects the electrical permittivity, especially when the ionic radius of the dopant significantly differs from the ionic radii of the base compound ions. However, in the case described in the article, this is not the case. The ionic radii of bismuth and gadolinium ions are comparable (see Table 1). Therefore, it can be postulated with a high probability that the changes in dielectric properties are due to changes in the microstructure caused by the introduction of the dopant. This statement is further supported by the lack of a clearly defined trend in these changes, which is probably a consequence not only of changes in the so-called average grain size but also of changes in the volume fraction of large grains compared to small grains. Confirmation of this thesis is provided by the ceramics containing the highest concentration of gadolinium ions. On one hand, it exhibits the highest dielectric permittivity, but on the other hand, it also shows an increase in grain size non-uniformity.

In order to compare the influence of gadolinium admixture on the properties of $\text{Bi}_7\text{Fe}_3\text{Ti}_3\text{O}_{21}$ ceramics, the temperature profiles of the real part of the electric permittivity measured at several selected frequencies of the measurement field were also analyzed (Figure 7).

Analyzing the above characteristics, it can be seen that there is no phase transition for all tested materials in the entire temperature range and that with the increase in the frequency of the measuring field f , the value of the maximum of the real part of the electric permittivity ϵ'_{max} decreases, while moving towards higher temperature values. The systematic shift of the maxima ϵ'_{max} in the direction of increasing temperature values (along with the strengthening of the frequency of the measurement field f) represents dielectric relaxation [27]. The literature data show that for Aurivillius phases, dipole disorder and relaxation properties are related to order errors in the sequence of perovskite-like layers. Further analyzing the characteristics from Figure 7, it is noticed that for low frequencies, with the increase in the content of gadolinium ions, the value of the real part of the electrical permittivity increases significantly (especially for the dopant $x = 0.6$). For high frequencies, the changes are small. In order to determine the quantitative impact of the gadolinium

admixture on the dispersion, both for the temperature and the dispersion of the real part of the permittivity, formulas $\Delta T_{max} = T_{max}(1000 \text{ kHz}) - T_{max}(1 \text{ kHz})$ and $\Delta \epsilon'_{max} = \epsilon'_{max}(1 \text{ kHz}) - \epsilon'_{max}(1000 \text{ Hz})$ were used. Table 5 summarizes the information read from the characteristics shown in Figure 7.

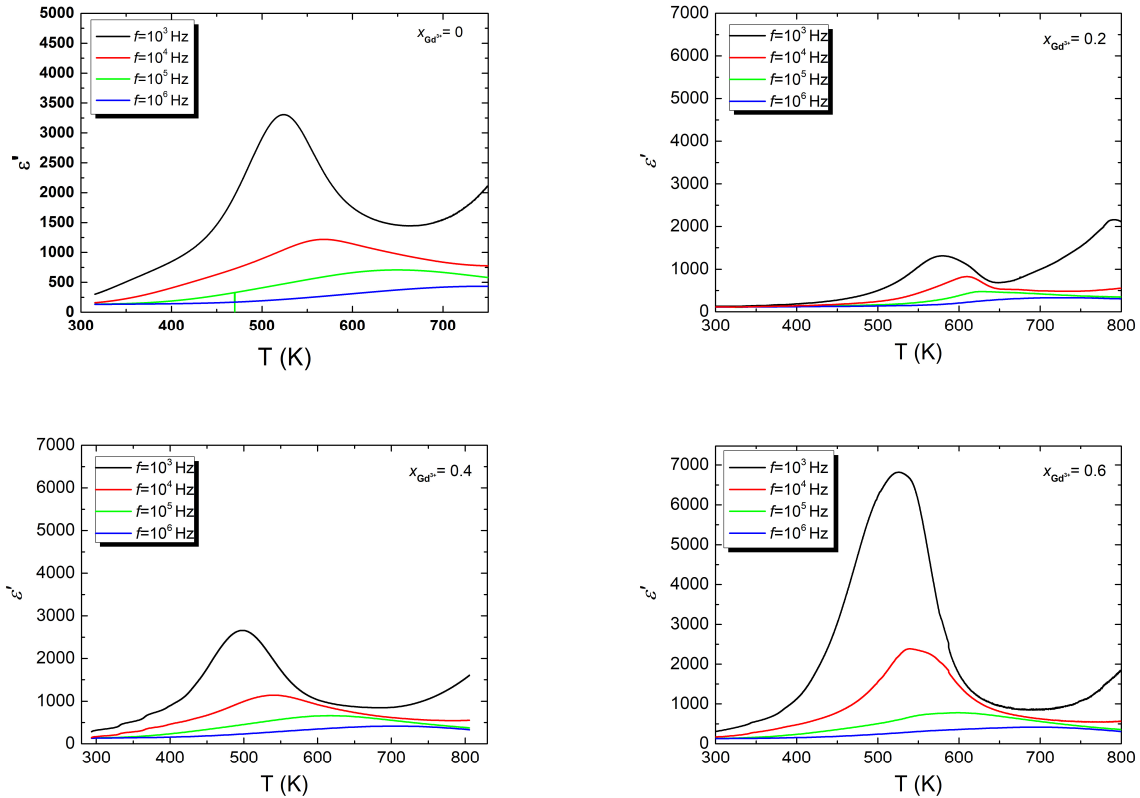


Figure 7. Temperature dependence of the real part of electric permittivity ϵ' for the $\text{Bi}_{7-x}\text{Gd}_x\text{Fe}_3\text{Ti}_3\text{O}_{21}$ ceramic materials for $x = (0, 0.2, 0.4, 0.6)$ in a measurement field with a frequency of $f = \{10^3, 10^4, 10^5, 10^6\}$ Hz.

Table 5. Degree of dispersion of $\Delta \epsilon'_{max}$ and ΔT_{max} for $\text{Bi}_{7-x}\text{Gd}_x\text{Fe}_3\text{Ti}_3\text{O}_{21}$ ceramic materials for $x = (0.2, 0.4, 0.6)$.

| | $\text{Bi}_{7-x}\text{Gd}_x\text{Fe}_3\text{Ti}_3\text{O}_{21}$ | |
|------------|---|----------------------|
| | $\Delta \epsilon'_{max}$ | ΔT_{max} [K] |
| 0.2 | 982 | 149 |
| 0.4 | 2258 | 207 |
| 0.6 | 6417 | 167 |

Although there is a minimum on the $\epsilon'(T)$ curves, the value of which depends on the frequency, the corresponding temperature does not shift to higher values with the increase in the frequency of the measurement field. This fact is most likely related to the decrease in the space charge density caused by the introduction of a homovalent dopant.

3.4. The Magnetoelectric Effect

To investigate the magnetoelectric effect, a previously developed method was used, which was described in the publication [28]. The multiferroic magnetoelectric material can be treated as a system composed of two subsystems, namely, a magnetic subsystem and an electric subsystem. The coupling between these subsystems can be treated and described as a certain type of interaction energy.

The Hamiltonian of the magnetoelectric system can be presented in the form proposed by Alcantara and Gehring [29–31]. This Hamiltonian consists of three parts, namely (2)

$$H = H^m + H^e + H^{me} \tag{2}$$

where H^m is the Hamiltonian of the magnetic subsystem, H^e is the Hamiltonian of the ferroelectric subsystem, and H^{me} is the coupling interaction between the two subsystems. In the mean-field approximation, the electric permittivity can be written using the following relationship (3)

$$\varepsilon(T) = \varepsilon_0(1 + \alpha \langle S_i S_j \rangle) \tag{3}$$

where ε_0 is the electric permittivity of free space, α is the magnetoelectric coupling coefficient, and $S_i S_j$ is the spin–pair correlation.

The thermodynamic statistics can be used to receive the average value of the spin–pair correlation. It can be approximately obtained in the following (4):

$$\langle S_i \rangle = \frac{4e^{4\beta D} \sinh(2\beta \tilde{h}) + 2e^{\beta D} \sinh(\beta \tilde{h})}{1 + 2e^{4\beta D} \cosh(2\beta \tilde{h}) + 2e^{\beta D} \cosh(\beta \tilde{h})}, \tag{4}$$

where $\langle S_i S_j \rangle \approx \langle S_i \rangle \langle S_j \rangle$, $\beta = 1/k_B T$, k_B is the Boltzmann constant, D is the uniaxial single-ion anisotropy constant, and \tilde{h} is the effective mean field acting on the magnetic subsystem. Using Formulas (3) and (4), and the results of measurements of temperature dependences of electric permittivity, it is possible to calculate the values of the magnetoelectric coupling coefficient α , which is a measure of the magnetoelectric effect.

The magnetoelectric coupling coefficient was calculated for undoped multiferroic Aurivillius-type material with chemical formula $\text{Bi}_7\text{Fe}_3\text{Ti}_3\text{O}_{21}$ (Figure 8a) and for doped Aurivillius-type material with gadolinium ions (Gd^{3+}) with chemical formula $\text{Bi}_{7-x}\text{Gd}_x\text{Fe}_3\text{Ti}_3\text{O}_{21}$ for $x = 0.2; 0.4; 0.6$ (Figure 8b–d respectively).

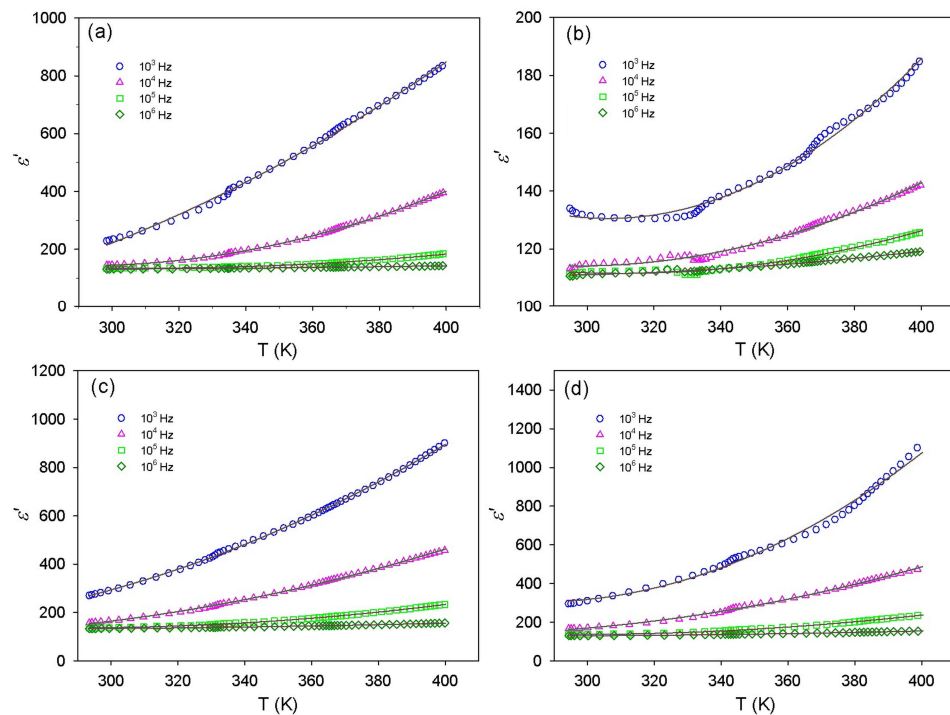


Figure 8. Temperature dependences of electrical permittivity for the undoped material (a) and for the doped with gadolinium ions, materials: $x = 0.2$ (b), $x = 0.4$ (c), $x = 0.6$ (d). Solid lines (in all figures) indicate curves obtained from fitting.

The calculated values of the magnetoelectric coupling coefficient α are listed in Table 6. The weakest magnetoelectric effect is observed in the material doped with gadolinium ions in the amount of $x = 0.6$ at a frequency of $f = 1$ kHz. The value of the magnetoelectric coupling coefficient α for this material is equal to $1.28 \cdot 10^{-9}$ s/m. At the same time, the strongest magnetoelectric effect occurs in the material doped with gadolinium ions in the amount of $x = 0.2$ at a frequency of $f = 1$ MHz, for which the value of the magnetoelectric coupling coefficient α is equal to $12.58 \cdot 10^{-9}$ s/m. The obtained coupling coefficient values are comparable to the literature data for analogous Aurivillius-type materials, for which the magnetoelectric coupling coefficient is of the order of $10^{-9} \div 10^{-7}$ s/m [6,32].

Table 6. Values of the magnetoelectric coupling coefficient α , calculated for undoped and doped with Gd^{3+} ions multiferroic Aurivillius-type material and for several frequencies of the electric measurement field.

| | 1000 Hz | 10,000 Hz | 100,000 Hz | 1,000,000 Hz |
|----------------|---------------------------|-----------|------------|--------------|
| Gd^{3+} ions | α [10^{-9} s/m] | | | |
| $x = 0$ | 1.49 | 3.49 | 5.22 | 8.62 |
| $x = 0.2$ | 9.28 | 11.73 | 11.45 | 12.58 |
| $x = 0.4$ | 1.50 | 2.97 | 7.00 | 9.80 |
| $x = 0.6$ | 1.28 | 2.85 | 6.93 | 10.24 |

Application considerations require that the multiferroic material exhibits the strongest possible magnetoelectric effect in the widest possible frequency range. Therefore, further work will be carried out to improve the technological process and select the appropriate quantity and type of dopant ions to obtain the strongest possible magnetoelectric coupling between electric and magnetic properties.

4. Conclusions

The BGFT- x ($x = 0; 0.2; 0.4; 0.6$) research material was successfully obtained as a result of a solid-state synthesis reaction by free sintering in an air atmosphere. The X-ray diffraction (XRD), microstructure (SEM, EDS), dielectric properties, and magnetoelectric effect of obtained ceramics have been studied. The XRD results show the BGFT- x ceramics are single-phase with an orthorhombic structure with the $Fm2m$ space group. SEM images have shown that doping the base material with gadolinium ions Gd^{3+} causes changes in the microstructure, namely, the shape of the plate-like grains changes to rounded. As the admixture grows, large plates begin to appear, but they are few in number compared to the rest of the grains. EDS analysis confirmed the obtained ceramics' qualitative and quantitative chemical composition and excluded the involvement of foreign elements or possible impurities. Dielectric measurements have shown that the admixture of gadolinium ions affects the electric permittivity values, in particular, its maximum value and the temperature at which this value occurs. Frequency-dependent characteristics of electric permittivity have revealed the presence of strong relaxation, which can be associated with the characteristic disorder of dipoles in the Aurivillius phase and with ordering errors in the sequence of perovskite-like layers. The study of the magnetoelectric effect by calculating the magnetoelectric coupling coefficient α shows that the magnitude of the magnetoelectric effect depends not only on the frequency of the electric measurement field but also on the amount of gadolinium ions added. The strongest coupling effect is demonstrated by material BGFT- x with $x = 0.2$.

Author Contributions: Conceptualization, M.A.-H.; methodology, D.S. and K.O.; software, M.C. and M.A.-H., validation, M.A.-H.; formal analysis, M.A.-H. and J.A.B.; investigation, D.S.; resources, M.A.-H.; data curation, J.M.; writing—original draft preparation, D.S.; writing—review and editing, J.M.; visualization, M.C., M.A.-H., J.M. and J.A.B.; supervision, M.A.-H.; project administration,

M.A.-H.; funding acquisition, M.A.-H. All authors have read and agreed to the published version of the manuscript.

Funding: This research received no external funding.

Institutional Review Board Statement: Not applicable.

Informed Consent Statement: Not applicable.

Data Availability Statement: Data are contained within the article.

Conflicts of Interest: The authors declare no conflicts of interest.

References

1. Béa, H.; Gajek, M.; Bibes, M.; Barthélémy, A. Spintronics with multiferroics. *J. Phys. Condens. Matter* **2008**, *20*, 434221–434232. [[CrossRef](#)]
2. Bibes, M.; Barthélémy, A. Oxide Spintronics. *IEEE Trans. Electron Devices* **2007**, *54*, 1003–1023. [[CrossRef](#)]
3. Liang, X.; Chen, H.; Sun, N.X. Magnetoelectric materials and devices. *APL Mater.* **2021**, *9*, 041114–041141. [[CrossRef](#)]
4. Liang, X.; Matyushov, A.; Hayes, P.; Schell, V.; Dong, C.; Chen, H.; He, Y.; Will-Cole, A.; Quandt, E.; Martins, P.; et al. Roadmap on Magnetoelectric Materials and Devices. *IEEE Trans. Magn.* **2021**, *57*, 400157. [[CrossRef](#)]
5. Yakout, S.M. Spintronics: Future Technology for New Data Storage and Communication Devices. *J. Supercond. Nov. Magn.* **2020**, *33*, 2557–2580. [[CrossRef](#)]
6. Faraz, A.; Arif, S. Magnetic-field-induced ferroelectric domain dynamics and in-plane polarization in odd and mixed layered Aurivillius structures. *J. Appl. Phys.* **2019**, *126*, 084104. [[CrossRef](#)]
7. Liu, Z.; Chen, F.; Gao, Y.; Liu, Y.; Fang, P.; Wang, S. A novel synthetic route for magnetically retrievable Bi₂WO₆ hierarchical microspheres with enhanced visible photocatalytic performance. *J. Mater. Chem. A* **2013**, *1*, 7027–7030. [[CrossRef](#)]
8. Zhang, Y.; Schultz, A.M.; Salvador, P.A.; Rohrer, G.S. Spatially selective visible light photocatalytic activity of TiO₂/BiFeO₃ heterostructures. *J. Mater. Chem.* **2011**, *21*, 4168–4174. [[CrossRef](#)]
9. Guo, R.; Fang, L.; Dong, W.; Zheng, F.; Shen, M. Magnetically separable BiFeO₃ nanoparticles with a γ -Fe₂O₃ parasitic phase: Controlled fabrication and enhanced visible-light photocatalytic activity. *J. Mater. Chem.* **2011**, *21*, 18645–18652. [[CrossRef](#)]
10. Li, X.; Ju, Z.; Li, F.; Huang, Y.; Xie, Y.; Fu, Z.; Knized, R.J.; Lu, Y. Visible light responsive Bi₇Fe₃Ti₃O₂₁ nanoshelf photocatalysts with ferroelectricity and ferromagnetism. *J. Mater. Chem. A* **2014**, *2*, 13366–13372. [[CrossRef](#)]
11. Eerenstein, W.; Mathur, N.D.; Scott, J.F. Multiferroic and magnetoelectric materials. *Nature* **2006**, *442*, 759–765. [[CrossRef](#)] [[PubMed](#)]
12. Veenachary, V.V.; Ramana, E.V.; Babu, S.N.; Puli, V.S.; Saha, S.; Srinivasan, G.; Prasad, G.; Prasad, N.V. Magnetoelectric Properties of Aurivillius-Layered Perovskites. *Crystals* **2024**, *14*, 299. [[CrossRef](#)]
13. Sun, S.; Liu, C.; Wang, G.; Chen, Z.; Chen, T.; Peng, R.; Lu, Y. Structural and Physical Properties of Mixed-Layer Aurivillius-Type Multiferroics. *J. Am. Ceram. Soc.* **2016**, *99*, 3033–3038. [[CrossRef](#)]
14. Lisnevskaya, I.V.; Butova, V.V.; Rusalev, Y.V.; Shapovalov, V.V.; Zahran, H.Y.; Yahia, I.S.; Soldatov, A.V. The effect of heterovalent doping on the stability and properties of multiferroic Aurivillius phases. *Appl. Phys. A* **2020**, *126*, 168. [[CrossRef](#)]
15. Frit, B.; Mercurio, J.P. The crystal chemistry and dielectric properties of the Aurivillius family of complex bismuth oxides with perovskite-like layered structures. *J. Alloys Compd.* **1992**, *188*, 27–35. [[CrossRef](#)]
16. Kennedy, B.J.; Kubota, Y.; Hunter, B.A.; Ismunandar; Kato, K. Structural phase transitions in the layered bismuth oxide Ba-Bi₄Ti₄O₁₅. *Solid State Commun.* **2003**, *126*, 653–658. [[CrossRef](#)]
17. Achary, S.N.; Patwe, S.J.; Krishna, P.S.R.; Shinde, A.B.; Tyagi, A.K. Cation disorder and structural studies on Bi_{4-x}Nd_xTi₃O₁₂ (0.0 ≤ x ≤ 2.0). *Pramana* **2008**, *71*, 935–940. [[CrossRef](#)]
18. Zhang, Z.; Yan, H.; Dong, X.; Wang, Y. Preparation and electrical properties of bismuth layer-structured ceramic BiFDNbOg solid solution. *Mater. Res. Bull.* **2003**, *38*, 241–248. [[CrossRef](#)]
19. Shannon, R.D. Revised Effective Ionic Radii and Systematic Studies of Interatomic Distances in Halides and Chalcogenides. *Acta Cryst.* **1976**, *A32*, 751. [[CrossRef](#)]
20. Szalbot, D.; Bartkowska, J.A.; Adamczyk-Habrajska, M.; Chełkowska, G.; Pawełczyk, M.; Bara, M.; Dzik, J. Magnetoelectric properties of multiferroic Aurivillius type Bi₇Fe₃Ti₃O₂₁ ceramics. *Process. Appl. Ceram.* **2020**, *14*, 218–222. [[CrossRef](#)]
21. Szalbot, D.; Bartkowska, J.A.; Feliksik, K.; Bara, M.; Chrunik, M.; Adamczyk-Habrajska, M. Correlation between structure, microstructure, and dielectric properties of Bi₇Fe₃Ti₃O₂₁ ceramics obtained in different conditions. *Arch. Metall. Mater.* **2020**, *65*, 879–884. [[CrossRef](#)]
22. Rietveld, H.M. A Profile Refinement Method for Nuclear and Magnetic Structures. *J. Appl. Crystallogr.* **1969**, *2*, 65–71. [[CrossRef](#)]
23. Krzhizhanovskaya, M.; Filatov, S.; Gusarov, V.; Paufler, P.; Bubnova, R.; Morozov, M.; Meyer, D.C. Aurivillius phases in the Bi₄Ti₃O₁₂/BiFeO₃ system: Thermal behaviour and crystal structure. *Z. Anorg. Allg. Chem.* **2005**, *631*, 1603–1608. [[CrossRef](#)]
24. Patterson, A.L. The Scherrer Formula for X-ray Particle Size Determination. *Phys. Rev.* **1939**, *56*, 978. [[CrossRef](#)]
25. Kinoshita, K.; Yamaji, A. Grain-size effects on dielectric properties in barium-titanate ceramics. *J. Appl. Phys.* **1976**, *47*, 371–373. [[CrossRef](#)]

26. Ghayour, H.; Abdellahi, M. A brief review of the effect of grain size variation on the electrical properties of BaTiO₃-based ceramics. *Powder Technol.* **2016**, *292*, 84–93. [[CrossRef](#)]
27. Das, R.; Choudhary, R.N.P. Dielectric relaxation and magnetoelectric characteristics of lead-free double perovskite: Sm₂NiMnO₆. *J. Adv. Ceram.* **2019**, *8*, 174–185. [[CrossRef](#)]
28. Bartkowska, J.A.; Dercz, J. The determination of the magnetoelectric coupling coefficient from the temperature dependences of the dielectric permittivity for the multiferroic ceramics Bi₅Ti₃FeO₁₅. *J. Exp. Theor. Phys.* **2013**, *144*, 1004–1008. [[CrossRef](#)]
29. Alcantara, O.F.; Gehring, G.A. Magnetoelectric effect in antiferromagnetic crystals. *Adv. Phys.* **1980**, *29*, 731. [[CrossRef](#)]
30. Janssen, T.; Tjion, J.A. One-dimensional model for a crystal with displacive modulation. *Phys. Rev. B* **1981**, *24*, 2245. [[CrossRef](#)]
31. Gao, X.S.; Liu, J.M.; Li, Q.C.; Liu, Z.G. A Monte-Carlo study of magnetoelectric coupling system. *Ferroelectrics* **2001**, *252*, 69. [[CrossRef](#)]
32. Yu, Z.; Meng, X.; Zheng, Z.; Lu, Y.; Chen, H.; Huang, C.; Sun, H.; Liang, K.; Ma, Z.; Qi, Y.; et al. Room temperature multiferroic properties of rare-earth-substituted Aurivillius phase Bi₅Ti₃Fe_{0.7}Co_{0.3}O₁₅ ceramics. *Mater. Res. Bull.* **2019**, *115*, 235–241. [[CrossRef](#)]

Disclaimer/Publisher’s Note: The statements, opinions and data contained in all publications are solely those of the individual author(s) and contributor(s) and not of MDPI and/or the editor(s). MDPI and/or the editor(s) disclaim responsibility for any injury to people or property resulting from any ideas, methods, instructions or products referred to in the content.